PALEOCEANOGRAPHY, VOL. 28, 585–598, doi:10.1002/palo.20052, 2013

Southwest Pacific Ocean response to a warmer world: Insights from Marine Isotope Stage 5e

G. Cortese,[1] G. B. Dunbar,[2] L. Carter,[2] G. Scott,[1] H. Bostock,[3] M. Bowen,[4] M. Crundwell,[1] B. W. Hayward,[5] W. Howard,[6] J. I. Martínez,[7] A. Moy,[8,9] H. Neil,[3] A. Sabaa,[5] and A. Sturm[10]

Received 13 November 2012; revised 17 August 2013; accepted 5 September 2013; published 23 September 2013.

[1] Paleoceanographic archives derived from 17 marine sediment cores reconstruct the response of the Southwest Pacific Ocean to the peak interglacial, Marine Isotope Stage (MIS) 5e (ca. 125 ka). Paleo-Sea Surface Temperature (SST) estimates were obtained from the *Random Forest* model—an ensemble decision tree tool—applied to core-top planktonic foraminiferal faunas calibrated to modern SSTs. The reconstructed geographic pattern of the SST anomaly (maximum SST between 120 and 132 ka minus mean modern SST) seems to indicate how MIS 5e conditions were generally warmer in the Southwest Pacific, especially in the western Tasman Sea where a strengthened East Australian Current (EAC) likely extended subtropical influence to ca. 45°S off Tasmania. In contrast, the eastern Tasman Sea may have had a modest cooling except around 45°S. The observed pattern resembles that developing under the present warming trend in the region. An increase in wind stress curl over the modern South Pacific is hypothesized to have spun-up the South Pacific Subtropical Gyre, with concurrent increase in subtropical flow in the western boundary currents that include the EAC. However, warmer temperatures along the Subtropical Front and Campbell Plateau to the south suggest that the relative influence of the boundary inflows to eastern New Zealand may have differed in MIS 5e, and these currents may have followed different paths compared to today.

Citation: Cortese, G., et al. (2013), Southwest Pacific Ocean response to a warmer world: Insights from Marine Isotope Stage 5e, *Paleoceanography*, *28*, 585–598, doi:10.1002/palo.20052.

1. Introduction

[2] The Australian-New Zealand sector of the Southwest (SW) Pacific Ocean is a major confluence where tropical and subtropical surface waters meet and interact with waters of Subantarctic and Antarctic origins. The confluence is marked by the prominent Subtropical and Subantarctic Fronts and associated current systems, including the anticyclonic South Pacific Subtropical Gyre (SPG) in the north and the cyclonic Antarctic Circumpolar Current (ACC) in the south (Figure 1). Modern observations indicate that this highly dynamic region is undergoing change in response to a warming climate [*Toggweiler et al*., 2006; *Roemmich et al*., 2007; *Hill et al*., 2008; *Ridgway and Hill*, 2009], making it relevant to assess long-term changes in the ocean in the face of further warming. In order to do so, we turn to reconstructions of past warm periods, a practice that is well established in the literature. Here we use paleoceanographic archives derived from marine sediment cores to assess the response of the SW Pacific Ocean to the peak interglacial, Marine Isotope Stage (MIS) 5e centered on ca. 125 ka.

[3] We are mindful of the limitations of comparisons with past interglacial periods and in that context the choice of MIS 5e is a compromise. It is not a direct analogue for projecting the future of the present interglacial, MIS 1, due to differences in orbitally forced insolation. MIS 5e has prominent eccentricity and precessional components, whereas MIS 1, and its oft-quoted insolation analogue, MIS 11, are periods of low eccentricity and precessional influence [*Loutre and Berger*, 2003]. Even comparisons between MIS 1 and MIS

Additional supporting information may be found in the online version of this article.

[1]GNS Science, Lower Hutt, New Zealand.
[2]Antarctic Research Centre, Victoria University of Wellington, Wellington, New Zealand.
[3]National Institute of Water and Atmospheric Research (NIWA), Wellington, New Zealand.
[4]School of Environment, University of Auckland, Auckland, New Zealand.
[5]Geomarine Research, Auckland, New Zealand.
[6]Research School of Earth Sciences, Australian National University, Canberra, Australia.
[7]Ciencias del Mar, Department of Geology, Universidad EAFIT, Medellin, Colombia.
[8]Department of Sustainability, Environment, Water, Population, and Communities, Australian Antarctic Division, Kingston, Tasmania, Australia.
[9]Antarctic Climate and Ecosystems Cooperative Research Centre, University of Tasmania, Hobart, Australia.
[10]Alfred Wegener Institute for Polar and Marine Research, Bremerhaven, Germany.

Corresponding author: G. Cortese, GNS Science, PO Box 30368, Lower Hutt 5040, New Zealand. (g.cortese@gns.cri.nz)

©2013. American Geophysical Union. All Rights Reserved.
0883-8305/13/10.1002/palo.20052

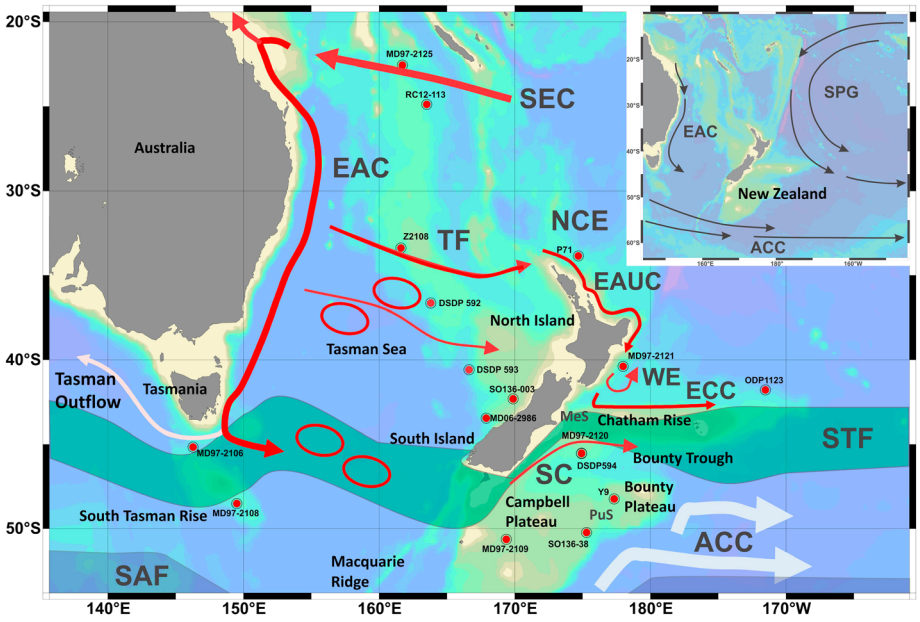

Figure 1. Map of core locations, approximate positions of main, modern warm currents, and other geographic and oceanographic features discussed in the text. The inset (top right) shows a simplified version of the large-scale circulation, with the position of the South Pacific Gyre (SPG), the Antarctic Circumpolar Current (ACC), and the East Australian Current (EAC). SEC = South Equatorial Current, EAC = East Australian Current, TF = Tasman Front, EAUC = East Auckland Current, SC = Southland Current, WE = Wairarapa Eddy, NCE = North Cape eddy region, PuS = Pukaki Saddle, MeS = Mernoo Saddle, ACC = Antarctic Circumpolar Current, STF = Subtropical Front, SAF = Subantarctic Front. Approximate front locations (for STF and SAF, shaded) are from *Orsi et al.* [1995], *Carter et al.* [1998], and *Orsi and Harris* [2001].

11 are open to question reflecting uncertainties regarding the roles of precession and obliquity [*Tzedakis*, 2010]. However, sediment cores containing MIS 5e (1) are more numerous than those containing MIS 11 and thus are more likely to provide the spatial coverage required to capture the changes in the oceanographically diverse SW Pacific Ocean and (2) MIS 5e is generally recognized as a period when global temperatures were 2–3°C warmer than present, a temperature range that may be reached within this century.

[4] Given the extent of the ACC and SPG [*Roemmich et al.*, 2007], the latter being part of an even larger southern "supergyre" [*Ridgway and Dunn*, 2007], this study has wide implications. Furthermore, because the study encompasses the southern midlatitudes, it provides insights into the long-term interaction of equatorial and polar signals in a region that is presently dominated by Southern Annular Mode (SAM) and El Niño-Southern Oscillation (ENSO) climate modes [*Carter et al.*, 2008].

[5] *CLIMAP* [1976] provided a first snapshot of the ocean during the Last Glacial Maximum (LGM), documenting the World Ocean Sea Surface Temperatures (SSTs) under full glacial conditions. This ambitious project went on to provide seasonal maps of the ocean during the LGM [*CLIMAP*, 1981], and a reconstruction [*CLIMAP*, 1984] of MIS 5e.

[6] However, these pioneering efforts to reconstruct the MIS 5e ocean suffered from several problems, including a lack of records from the SW Pacific, a limited choice of SST reconstruction techniques available at that time, discordances in the estimates obtained from different fossil groups [see *Howard and Prell*, 1984], inadequate knowledge of the depth and seasonal adaptations of those groups, and changes in the seasonality of the SST signal.

[7] To improve the quality and reliability of the reconstruction, a recent synthesis of LGM SSTs [*Kucera et al.*, 2005; *MARGO Project Members*, 2009] has adopted a multitechnique approach to regional calibration data sets. This reconstruction, derived from foraminiferal census data, was based on four different transfer function techniques applied to three regional calibration data sets for the North Atlantic, South Atlantic, and for the Pacific Ocean. Another broad-scale reconstruction, using diatom evidence to document the paleoclimate evolution of the Atlantic and western Indian sector of the Southern Ocean between MIS 6 and 5e, was generated by *Bianchi and Gersonde* [2002] and provided insights on the detailed SST evolution during Termination II and the important role sea-ice plays in triggering the early warming of the Southern Ocean at glacial terminations when compared to northern latitudes.

[8] Subsequent, more regional, studies have improved our knowledge of the paleoceanography of the SW Pacific region including the evolution of the resident ocean frontal systems [examples are: *Nelson et al.*, 1993, *Martinez*, 1994; *Sikes et al.*, 2002, 2009; *Neil et al.*, 2004; *Moy et al.*, 2006; *Nürnberg and Groeneveld*, 2006; *Barrows et al.*, 2007; *Carter et al.*, 2008; *Crundwell et al.*, 2008; *Hayward et al.*, 2008, 2012 and references therein]. These studies provide information on ocean change over glacial to interglacial cycles that relates to (i) migrations of ocean fronts and water masses, (ii) SSTs, and (iii) ocean circulation.

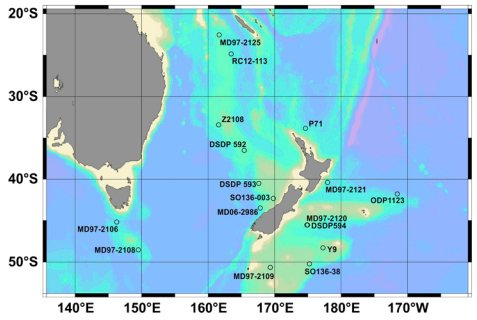

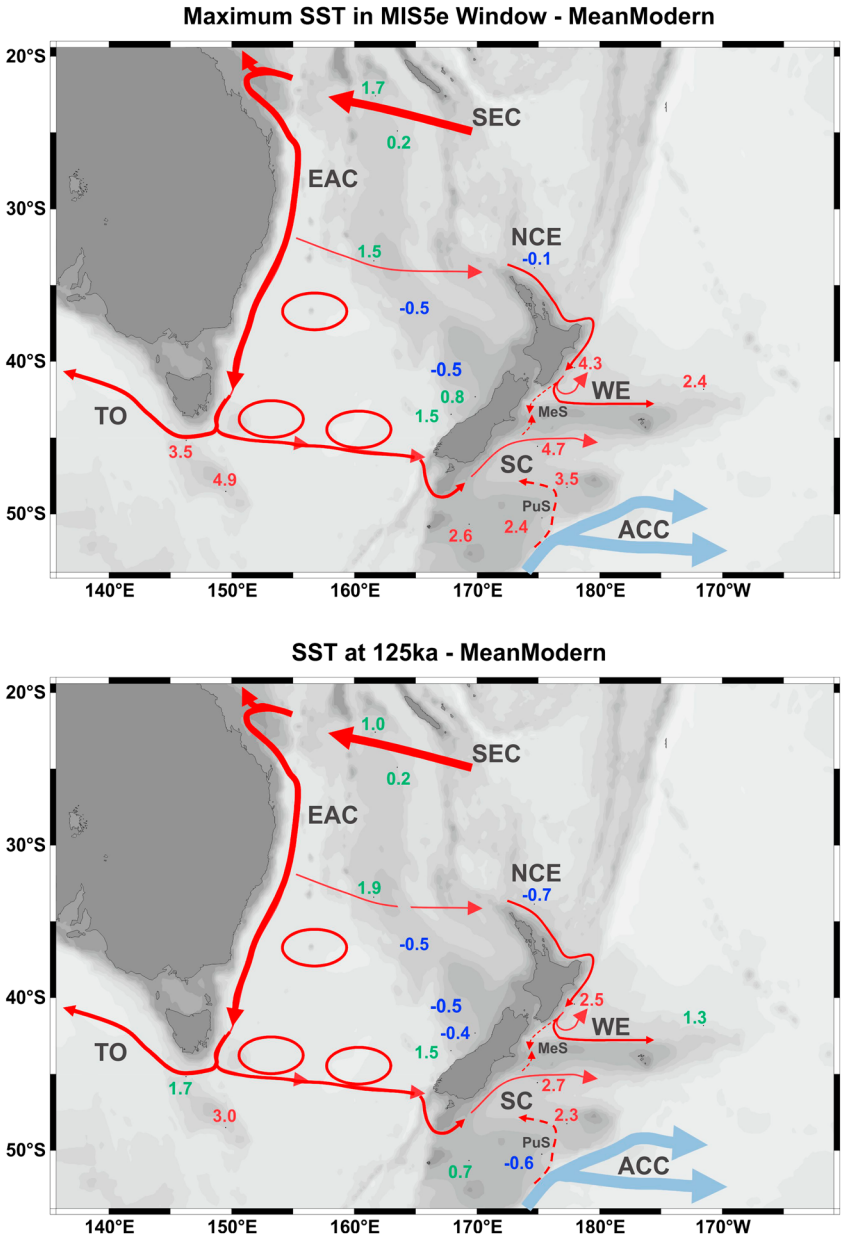

Figure 2. **Top Panel**: location of cores. **Middle Panel**: Map of SST anomalies in degrees centigrade (highest SST value recorded between 120 and 132 ka minus Modern mean annual SST) at the investigated sites (located in inset). The magnitude of the anomalies is color coded as blue (negative), green (0 to 2°C), and red (>2°C). Simplified surface currents inferred for MIS 5e are also shown, with the dotted arrows representing water exchanges across the Mernoo (MeS) and Pukaki (PuS) Saddles. **Bottom Panel**: Map of SST anomalies in degrees centigrade (SST value recorded at 125 ka minus Modern mean annual SST) at the investigated sites. The color coding is the same as in the middle panel. Generalized circulation and shortenings as in Figure 1.

[9] Our study, based on a full interglacial interval, attempts to overcome some of the limitations faced by the earlier efforts. Our choice of estimates derived from foraminiferal faunal data circumvents the discordances arising from comparing data derived from a variety of fossil groups. The single fossil group approach also reduces problems linked to the seasonality of the signal generation [e.g., *Sikes et al*., 2009]. In fact, efforts to map SST patterns at specific time slices, or to recognize temporal trends, are severely hampered when general conclusions are drawn from SSTs derived from mixed proxies. While this was recognized by *CLIMAP* [1984], *Leduc et al*. [2010] clearly illustrate this problem and its consequences on SST trends, even when using advanced biogeochemical methods for the reconstruction of past temperatures. In their study, foraminiferal Mg/Ca SST records often provided a different picture of Holocene SST evolution compared to those derived from alkenones. *Leduc et al*. [2010] interpret this difference as arising from the seasonal influence on the generation and storage of the paleotemperature signal between these two widely used methods. Moreover, their data suggest that the potential bias also influences SST reconstructions for MIS 5e and is hence a consideration for this study. In order to increase spatial coverage, we include the Mg/Ca record for site MD97-2125 [*Tachikawa et al*., 2009], from a region of low seasonal temperature variability and consistent with faunal data from the same region.

[10] We also include recent observations of SST and wind stress curl trends (over the past 30 and 60 years, respectively) to check for viable physical processes to explain the observed oceanographic changes during MIS 5e.

2. Oceanographic Setting

[11] The South Equatorial Current (SEC), the westward-flowing arm of the SPG, enters the region between 15°S and 20°S and separates into north and south flowing components approaching the east Australian continental margin (Figure 1). The latter flow continues as the eddy-rich East Australian Current (EAC), which is a western boundary current of the SPG [*Ridgway and Dunn*, 2003]. The EAC has essentially two outlets, which have similar mean volume transports of ca. 10 Sv ($1\ \mathrm{Sv} = 10^6 \mathrm{m}^3\mathrm{s}^{-1}$) and high decadal variability [*Ridgway et al*., 2008; *Hill et al*., 2011]. The first outlet is the Tasman Front, which detaches from the eastern margin of Australia around 33°S–35°S and meanders to northernmost New Zealand where it turns south as the East Auckland Current off eastern North Island [*Stanton et al*., 1997; *Hill et al*., 2011]. This flow continues as the East Cape Current bringing subtropical water to the Chatham Rise where it is steered east by the Rise's northern flank. The second outlet comprises a southward extension of the EAC that passes Tasmania at ca. 45°S where it bifurcates with one arm turning west to form the Tasman outflow and the other arm directed east to contribute to the Subtropical Front (STF).

[12] In addition to the subtropical input from the north via the Tasman Front and its extension down the eastern margin of the North Island, New Zealand also receives subtropical water from the south via the STF. This complex zone of interweaving subtropical (STW) and subantarctic (SAW) surface waters extends across the Tasman Sea from 45°S off Tasmania to 47°S–49°S off southernmost New Zealand. The STF zone is a double feature comprised of a shallow northern front that marks the northern limit of SAW, and a deeper southern front representing the poleward extent of STW [*Hamilton*, 2006]. Geostrophic transport is ca. 3Sv [*Stramma et al*., 1995] but approaching New Zealand, the southern STF intensifies along the eastern South Island margin where transport is 8–10 Sv northward to Chatham Rise [*Sutton*, 2003; *Smith et al*., 2013]. This so-called Southland Current was estimated to carry ~90% SAW on the basis of a "snapshot survey" by *Sutton* [2003]. However, an 8 year time series indicated alternating periods when either SAW or STW dominated the surface waters [*Sutton*, 2003; *Smith et al*., 2013]. Upon reaching the Chatham Rise, ca. 1.3 Sv leaks northward through the Mernoo Saddle to the eastern North Island, with most of Southland Current diverted east along the south-facing flank of the Rise (Figure 1).

[13] The dynamics of the southern study region are dominated by the mainly wind-driven ACC, in particular its northernmost boundary represented by the Subantarctic Front (SAF). This zonal jet has a mean volume transport of ca. 105 Sv south of Tasmania [*Rintoul and Sokolov*, 2001] and ca. 90 Sv along the eastern slope of the Campbell Plateau, but such averages belie a high variability [*Morris et al*., 2001]. Upon meeting Macquarie Ridge and Campbell Plateau, the SAF forms deep-reaching eddies that migrate along the steep plateau flanks to 55°S and 50°S [*Stanton and Morris*, 2004] before turning east near 49°S. However, the gap between Campbell and Bounty plateaux allows subpolar water to flow northward into the Bounty Trough and cyclonically around the Trough to bring cold subantarctic and circumpolar water to the southern Chatham Rise [*Davis*, 1998].

3. Methods

3.1. Definition of Time Slice and Chronology

[14] Regional syntheses of paleo-SST data usually focus on "snapshots" of time from widely spaced cores. Some level of interpolation, in space and time, of the proxy data is needed to generate the coverage required to identify regional variations especially in the diverse SW Pacific Ocean [e.g., *CLIMAP*, 1981, 1984; *Kucera et al*., 2005].

[15] Our approach is to place all records on a common timescale (supporting information Figure 2) by matching their benthic $\delta^{18}O$ time series to the LR04 benthic isotope stack [*Lisiecki and Raymo*, 2005] using the *Analyseries* software [*Paillard et al*., 1996]. We identify MIS 5e as the lightest benthic $\delta^{18}O$ value during 100–160 ka. Although we acknowledge that other alignment strategies may be equally valid, that period is deliberately broadly defined in order to accommodate different sampling resolutions and sedimentation rates between records and potential spatial variability in the timing of peak warmth within the study region. We then pick the highest SST value recorded between 120 and 132 ka and generate SST anomaly maps by subtracting the modern mean SST value for the core location from this value. In most cases, this will allow us to capture the peak SST value during MIS 5e, but for low sampling resolution the SSTs will be a minimum value because peak temperature may be unsampled.

[16] The alternative approach of calculating the anomaly by picking the SST value at the sample closest to 125 ka, and thus providing a synoptic SST picture for MIS 5e, is itself biased by the same uncertainties arising from variable

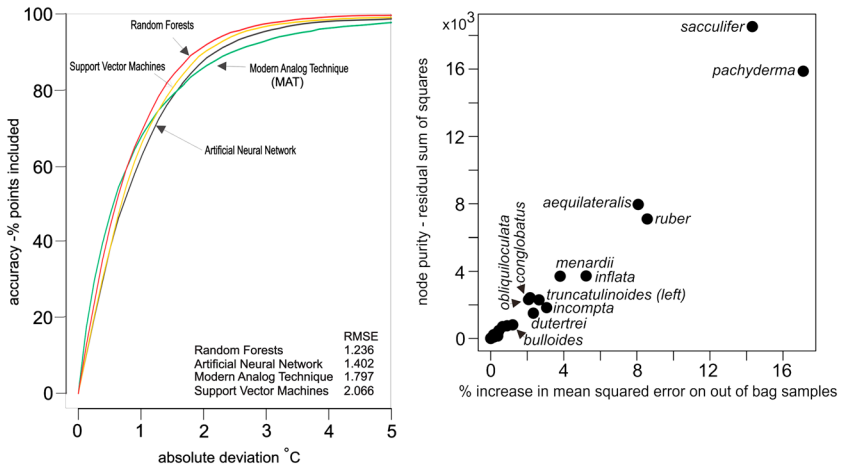

Figure 3. **Left Panel**: Regression error characteristic curves [*Bi and Bennett*, 2003] for models trained on the SH0911C2 database using R package *rminer* (available at http://cran.r-project.org/web/packages/rminer/). The percentage of the training set is plotted against error tolerance (SST °C). R functions used are kknn for MAT; nnet for Artificial Neural Network; ksvm for Support Vector Machines; randomForest for Random Forests. Root mean squared errors are listed. **Right Panel**: The *x* axis plots the average percent increase in mean squared error over all trees of a taxon when its OOB error (OOB = "out-of-bag" segment of data not used for training) is permutated and compared with the OOB error of the tree. This is a measure of the SST information carried by the taxon. The *y* axis plots node purity, estimated by residual sum of squares from splitting on each taxon averaged over all trees, as a measure of its importance for estimating SST.

sedimentation rates, sampling resolution, and age model accuracy between cores. The SST patterns obtained by applying both approaches are shown in Figure 2: as the general geographic pattern and the sign of the anomalies are essentially unchanged between the two, and thus the main conclusions of this study would not be affected, we discuss our findings on the basis of the "MIS 5e window" results. In this work, we synchronized the age models of our records based on the *Lisiecki and Raymo* [2005] benthic $\delta^{18}O$ stack, which has itself a stated age uncertainty, including all sources of error, of ~4 ka over last million years. Part of this uncertainty, due to the radiometric calibration of isotope events, amounts to ca. 1 ka for U/Th dating back to ca. 130 ka [*Thompson and Goldstein*, 2006], making discrete events within the last glacial-interglacial cycle, such as the peak sea level associated with MIS 5e somewhat better constrained. However, the uncertainties inherent in the LR04 $\delta^{18}O$ reference curve are compounded by a degree of subjectivity in the fit between our core $\delta^{18}O$ curves, especially where the sample resolution is not high, and the LR04 $\delta^{18}O$ stack. These uncertainties, coupled with the asynchronous character of SST change during MIS 5 [*Turney and Jones*, 2010], make the choice of a representative, specific and at the same time synoptic, stratigraphic horizon for MIS 5 problematic. A strategy commonly adopted in literature (see for example the recent data compilation for last interglacial by *Turney and Jones* [2010]) is to average the proxy SST data over a broader time slice, in order to minimize age model-related errors and at the same time capture a "steady-state" picture of SST conditions during MIS 5e, following the large oceanographic reorganizations occurring at Termination II. For this reason, and in order to be able to compare our data to the proxy compilation mentioned above, and the model intercomparison results of *Lunt et al*. [2013], we also provide an anomaly map (Figure 5) based on averaging SSTs in the 115 to 130 ka time slice (Table 2). A by-product of this approach is to provide a standard deviation for our SST proxy data, of the order of 1–2°C over this time interval. The general conclusions of this work (strong warming off Tasmania, warming in the EAC system and on the Campbell Plateau, cooling in the eastern Tasman Sea) are not particularly sensitive to the inevitable chronological uncertainties, and the SST anomaly pattern for the averaged time slice (Figure 5) is essentially the same as the one observed for the other two approaches mentioned above (Figure 2).

3.2. Paleotemperature Reconstructions

[17] Estimation of paleo-SST from faunal census data in core-top samples is performed via supervised learning methods. The primary step is to establish a relationship between faunal abundances (predictor variables) in a Holocene training set and modern SSTs (the known target variable) that can be used to estimate the paleo-SST of counterpart fossil faunas.

[18] Our training set (SH0911C2, available from http://www.ncdc.noaa.gov/paleo/paleo.html) augments that used by *Crundwell et al*. [2008, Figure 2] with additional data from *Mohtadi et al*. [2005; 2007], *MARGO Indo-Pacific dataset* (http://doi.pangaea.de/) and additional data [*Crundwell*, unpublished]. It includes 1223 Southern Hemisphere sites, whose geographic positions are shown in supporting information Figure 3, while taxa abundances at these locations are available in supporting information Table 1. The latter data are harmonized to 35 taxa (Table 1): nominally the counts are from the >149 μm size fraction, although we are not able to confirm this for all sites. Duplicate counts are averaged. Taxa include primarily near-surface dwellers through to globorotaliids, whose adults live below the thermocline. Most Southern Hemisphere water masses are sampled, although representations from the Southern Ocean and central Pacific are small (supporting information Figure 3).

Table 1. Basic Statistics (Localities at Which Taxon is Present, Maximum and Mean Abundance) for the Taxa Used in the Training Set[a]

SH0911C2 Taxa	Localities Present	Maximum Abundance	Mean
Beella digitata	641	13.51%	0.68%
Candeina nitida	159	27.21%	0.54%
Globigerina bulloides	1151	73.63%	11.08%
Globigerina falconensis	775	35.74%	3.25%
Globigerinella adamsi	99	8.34%	0.58%
Globigerinella aequilateralis	886	16.92%	3.73%
Globigerinella calida	792	9.07%	1.92%
Globigerinita glutinata	1120	91.56%	8.82%
Globigerinita iota	50	4.95%	0.55%
Globigerinita uvula	21	2.10%	0.40%
Globigerinoides conglobatus	658	42.67%	2.24%
Globigerinoides ruber	968	72.06%	21.48%
Globigerinoides sacculifer	876	38.75%	8.12%
Globigerinoides tenellus	566	9.93%	1.71%
Globoconella inflata	808	80.08%	15.38%
Globoquadrina conglomerata	315	12.66%	1.90%
Globorotaloides hexagona	298	9.44%	1.02%
Hirsutella hirsuta	364	8.69%	1.22%
Hirsutella scitula	518	7.23%	0.75%
Hirsutella theyeri	30	1.14%	0.47%
Menardella menardii	668	60.12%	7.60%
Neogloboquadrina dutertrei	1036	96.39%	11.18%
Neogloboquadrina incompta	926	91.00%	10.50%
Neogloboquadrina pachyderma	519	100.00%	18.42%
Orbulina universa	884	32.73%	1.27%
Pulleniatina obliquiloculata	701	88.54%	5.86%
Sphaeroidinella dehiscens	334	13.12%	0.75%
Tenuitella anfracta	17	0.45%	0.24%
Truncorotalia crassaformis	389	13.98%	1.17%
Truncorotalia crassula	136	4.60%	0.58%
Truncorotalia truncatulinoides (*dextral*)	486	10.99%	1.70%
Truncorotalia truncatulinoides (*sinistral*)	601	17.98%	3.28%
Turborotalita humilis	126	2.74%	0.48%
Turborotalita quinqueloba	480	35.71%	3.51%
Zeaglobigerina rubescens	523	7.80%	1.32%

[a]Detailed abundance data are available in supporting information Table 1.

The target variable is mean annual surface ocean temperature from the CSIRO Atlas of Regional Seas 2009 (CARS) [*Ridgway et al*., 2002]. CARS includes data from the World Ocean Atlas but interpolates it to a finer grid (0.5°) than WOA with a method that better resolves the influence of complex topography and land barriers on the flows in this region [*Ridgway and Dunn*, 2003]. Surface mean ocean temperature from CARS is interpolated to each core location.

3.2.1. Comparison of Learning Techniques

[19] In their pioneering study on prediction of paleo-SST from Holocene distributions of planktonic foraminifera for CLIMAP, *Imbrie and Kipp* [1971] used factor analysis to reduce the number of predictor variables (species abundances), which were then regressed linearly on modern SSTs. *Hutson* [1980] introduced a nearest-neighbor clustering method, the modern analog technique (MAT), to predict paleo-SST from a fossil fauna by its statistical distance (assemblage dissimilarity) from core-top faunas (modern analogues). This simple nonparametric method, along with its variants [*Malmgren et al*., 2001], is very widely applied in paleo-environmental studies [*Theron et al*., 2004; *Birks et al*., 2010]. *Malmgren and Nordlund* [1997] showed that artificial neural networks, which are two-stage nonlinear regression models, out-performed these earlier methods.

[20] In view of the spectrum of learning techniques now available [*Hastie et al*., 2009], we used the software package rminer [*Cortez*, 2010; available at: http://cran.r-project.org/web/packages/rminer/index.html)] to evaluate the performance of several methods for predicting paleo-SST by comparing their regression error characteristic curves (REC) [*Bi and Bennett*, 2003] for the SH0911C2 training set. REC curves plot error tolerance against accuracy of a regression, where accuracy is the percentage of points fitted within a specified tolerance interval. The ideal curve is a vertical line against the ordinate axis which represents exact matches between observed and predicted SST. For an error tolerance of 0–1°C, the MAT method (Figure 3) is the best predictor, followed by Random Forests. For larger error tolerances, MAT is replaced by Random Forests which, over the full training set, is the best predictor (Figure 3).

3.2.2. Application of Random Forests Learning

[21] Random Forests [*Breiman*, 2001] uses recursive binary splitting to build a regression tree. Starting at the root node, which is a bootstrap sample of the same size as the original data, a preset number of randomly selected training variables is searched for the best split into two child nodes, as measured by the mean squared error of the target variable. Binary splitting of nodes using randomly selected variables continues until the largest tree possible is built. A large number of such decorrelated trees are grown to create an ensemble. Prediction is achieved by feeding new data through each of the trees and averaging the outputs to reduce their variance. The method is detailed by *Liaw and Wiener* [2002] and *Hastie et al*. [2009]. It is nonparametric, robust to overfitting, and resistant to outliers. An ensemble of 500 trees from the SH0911C2 training set was computed using the Random Forest package (http://cran.r-project.org/web/packages/randomForest/). The 95% confidence interval for each predicted SST, computed from the 500 estimates, is shown in supporting information Figure 2. The 95% confidence interval for the mean was calculated as: 95% CI = $x \pm t_{crit}$ * (σ/sqrt (n)), where x = the average SST (for each sample, this average is based on the values provided by the 500 Random Forests trees we generated); σ = the standard deviation of this average; the t_{crit} value (obtained from a table of the t distribution, based on a 95% confidence level, two tails, for 499° of freedom, corresponding to 1.96), and the square root of n = the number of observations (in our case 22.36, which is the square root of 500).

[22] The node purity (residual variance as measure of relationship) and the out-of-bag error (segment of training set not used for bootstrapping) are both plotted in Figure 3, as measures of variable importance. Both identify *Globigerinoides sacculifer* and *Neogloboquadrina pachyderma* as the most important taxa in the paleo-SST model. The former species is largely confined to tropical water masses [*Bé*, 1977] and the latter to subpolar-polar water masses. They dwell primarily in the mixed layer and their relative abundances are SST related. Of lesser importance are other mixed layer taxa: *Globigerinoides ruber* (a major tropical species) and *Globigerinella siphonifera*, a minor taxon which is widely distributed in Southern Hemisphere subtropical water [*Bé*, 1977]. Taxa with some adults living below the thermocline (*Globorotalia menardii*, *Globorotalia inflata*) carry more SST information than does *Globigerina bulloides*, whose abundance tends to be related to mixed layer productivity. In overview, the regression tree is primarily based on two taxa with quite distinct biogeographies. Several other important

taxa primarily dwell in the mixed layer, but there is some residual SST information in taxa with deeper-dwelling adults. Over 20 taxa provide little temperature information.

4. Results

4.1. Observed Changes in SST

[23] A regional map of the differences between the peak SST within the 120–132 ka window and today's modern mean annual SST shows a distinct spatial pattern with MIS 5e SST anomalies of between −0.5 and +1.9°C compared to their modern equivalents north of the STF (plotted in Figure 2 middle panel, all data available in supporting information Tables 2 and 3). In particular, the eastern and northern Tasman Sea shows little evidence of warmer SSTs during MIS 5e, and in some cases (DSDP 592/593, P71) small negative anomalies also occur. In contrast, MIS 5e SSTs in the STF zone and further south are between 2.3 and 4.9°C warmer. Particularly high anomalies (>3°C) occur to the east of New Zealand, in the Bounty Trough region (DSDP 594) and along the Tasman Rise southeast of Tasmania (MD97-2106; MD97-2108).

[24] The SST shift from full glacial to interglacial conditions also displays substantial variability (supporting information Figure 2). ODP 1123, DSDP 594, MD97-2106, and Y9 display sharp SST rises of ca. 7 to 12°C, MD97-2108 and Z2108 from the Tasman Sea exhibit moderate excursions of 3 to 4°C, and MD97-2109 has a subdued rise, ca. 2°C.

5. Discussion

[25] Upper ocean temperatures at any location are the result of heat flux from the atmosphere into the surface of the ocean, vertical entrainment of deeper water, and lateral advection of heat by currents. The relative influence of these processes on SST change is poorly quantified, even under modern conditions [e.g., discussion in *Gille*, 2008].

[26] Advection is most likely the main control of temperature at the sites close to the East Australian, East Auckland, and East Cape Currents, which are the western boundary currents of the STG. These currents are robust features of the ocean circulation [see idealized model experiments of *Tilburg et al*., 2001], whose present mean transport corresponds to the estimated wind-driven Sverdrup transport [*Stanton*, 2001]. Therefore, we interpret temperature anomalies at sites near these currents as due to differences in either the heat transport or circulation path of these currents.

[27] Sites with large positive anomalies south of 40°S (2.4 to 4.9°C) are also near the boundaries between subtropical and subantarctic waters where changes in currents and associated eddies are likely to cause large temperature changes, due to the presence of strong SST gradients compared to other oceanic regions. We interpret these large positive SST anomalies as caused by a different current pattern during MIS 5e compared to modern.

[28] Our MIS 5e data coverage of the SW Pacific is larger than that previously available. The magnitude of warming within our study area is consistent with the reconstructions of *Bianchi and Gersonde* [2002] for the last interglacial "climate optimum" period between 40°S and 55°S in the Indian and South Atlantic Oceans.

5.1. Regional Distribution of SSTs

[29] The geographic pattern of the SST anomalies between MIS 5e and today includes regions of (i) markedly warmer MIS 5e SSTs (anomalies >3°C) off the eastern South Island and central North Island plus South Tasman Rise; (ii) slightly cooler or warmer anomalies of −0.5 to +1°C, including most of the eastern Tasman Sea and northernmost New Zealand, and (iii) moderate warming (<2.5°C) on Campbell Plateau. The changes observed during MIS 5e are even more dramatic than those in modern times, with subtropical water likely affecting subantarctic locations.

[30] The warming of up to 4.9°C over South Tasman Rise is of the same order of magnitude as changes observed over the past six decades. Strengthening of the South Pacific Gyre has enhanced the EAC, which has extended 350 km southward past Tasmania [Figure 1: *Roemmich et al*., 2007; *Hill et al*., 2008, 2011]. As a result, southern EAC waters have warmed at a rate of 2.28°C/century, increased their salinity by 0.34/century, and caused subtropical biota to extend their ranges poleward [*Hill et al*., 2008; *Ridgway and Hill*, 2009]. Atmospheric and oceanic observations document a continued strengthening of the EAC, possibly at the expense of the Tasman Front, whose volume transport is projected to decline if current trends continue [*Cai et al*., 2005; *Sasaki et al*., 2008; *Hill et al*., 2011]. In these studies, the underlying mechanisms behind the observed trends are used to predict future change. The observed modern intensification of the EAC is matched by published paleoceanographic data, which consistently highlight southward migrations of the Subtropical Front both in the Southern Indian Ocean and along the south coast of Australia/around Tasmania during peak interglacial periods, such as MIS 5e or the early Holocene [e.g., *Howard and Prell*, 1992; *Martinez*, 1994; *Sikes et al*., 2009].

[31] The SST anomaly we observe (Figure 2, middle) at Z2108 (1.5°C) is likely closely related to the temperatures in the East Australian Current due to the EAC eddies that tend to fill the basin between the Australian coast and the Lord Howe Rise. Altimeter data show that present strong eddy activity is not found much further south than this location [*Tilburg et al*., 2001; *Bowen et al*., 2005]. The modern eddy kinetic energy (EKE) suggests the more southern DSDP 592 location receives less direct heat transport from EAC, consistent with the small negative SST anomaly (−0.5°C) observed there.

[32] The East Auckland Current is weaker when the EAC is stronger [*Cai et al*., 2005; *Hill et al*., 2011], which implies less heat transport into the North Cape eddy (NCE) region and lower temperatures there. During MIS 5e, this mechanism may have resulted in the small negative anomaly observed in the NCE region. Small anomalies (−0.5 to 0.8°C) are found off western New Zealand in the northeastern Tasman Sea, where persistent flows are very weak. The small anomalies suggest that trans-Tasman heat transport from the EAC is not large enough to dominate the SST in this region. By contrast, SSTs off southwestern New Zealand are warmer (1.5°C at MD06-2986), possibly due to a southward extension of the EAC [*Hill et al*., 2008] with correspondingly higher temperatures in the general region of the STF [cf. *Bianchi and Gersonde*, 2002].

[33] MIS 5e SST anomalies are much warmer in the Bounty Trough and Campbell Plateau (2–4°C). This region is the western boundary of the South Pacific and is characterized by strong currents that follow steep bathymetric contours [*Tilburg et al*.,

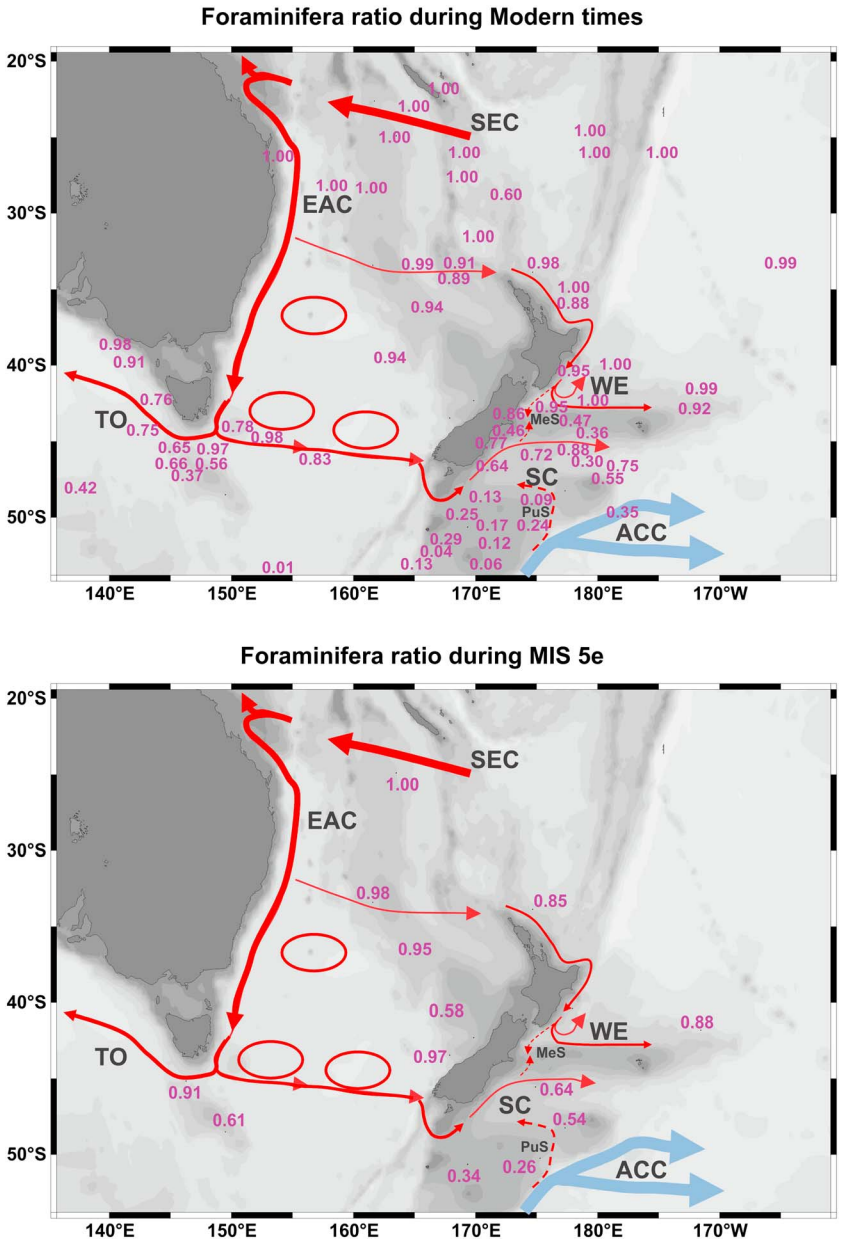

Figure 4. Ratios of (**Top Panel**) modern and (**Bottom Panel**) MIS 5e abundances of the foraminiferal planktic species expressed as (*Neogloboquadrina incompta*/(*N. incompta* + *N. pachyderma*)). The ratio is used to assess the relative contribution of subtropical versus subantarctic water masses at the various locations, with ratios close to unity being indicative of a subtropical affinity. Note, for clarity only those sites where the sum of *N. incompta* + *N. pachyderma* >5% is shown for the modern setting. Also to improve clarity, data from two sites on the South Tasman Rise, eight sites from the densely sampled Chatham Rise and the Campbell Plateau, and two from the Hikurangi Trough are omitted.

2001; *Sutton*, 2003]. These currents largely control surface temperatures in the region [as evinced in SST imagery, cf. *Uddstrom and Oien*, 1999] suggesting that the anomalies reflect changes either in the currents or in the temperature of water in the currents. The Southland Current presently brings < 1 Sv of subtropical water to eastern New Zealand [*Sutton*, 2003]: an increase in transport of subtropical water or an increase in the southern Tasman Sea temperatures would increase temperatures off the east coast of the South Island. An increase in temperatures of subantarctic waters would also contribute to warm the Bounty Trough.

[34] With that thought in mind, we turn to the Bounty Trough and its strong anomalies (>2°C)—a warming that can be attributed to some combination of the following mechanisms: (i) As noted previously, warmed Subantarctic surface and deeper waters could be introduced by the Southland Current reflecting the marked warming of the Southern Ocean with the upper 100 m rising by ca. 1.0°C for summer months since the 1930s and the interior at 700–1100 m by 0.17°C in the 1950s to 1980s [*Gille*, 2002, 2008]; (ii) Warm subantarctic and deeper waters from the Subantarctic Front of the ACC flow into the Bounty Trough via the 1400 m deep

Pukaki Saddle at 50°S [e.g., *Davis*, 1998; *Morris et al*., 2001]: Core Y9 on the eastern side of the Saddle exhibits an anomaly of 3.9°C and SO136-38 in the western approaches to the Saddle has a slightly cooler anomaly of 2.4°C; (iii) Transport of subtropical surface water from the north via Mernoo Saddle is another mechanism, which *Hayward et al*. [2008] invoked to account for the high SSTs estimated from foraminiferal transfer functions for MIS 5e. Southward transport is observed mainly during austral winter and spring and may be related to transient warm water eddies blocking and feeding the northern approach to Mernoo Saddle [*Greig and Gilmour*, 1992; *Shaw and Vennell*, 2000].

[35] Of the three proposed mechanisms, modern volume transports suggest that the largest heat contribution to the Bounty Trough comes from the Southland Current/STF, which has a mean transport of 8.3 Sv [*Sutton*, 2003]. Taking the cross-sectional area of Mernoo Saddle bounded by the 100 m isobath and a net northward flow of 3.1 cm/s [*Greig and Gilmour*, 1992], we estimate that ca. 1.3 Sv escapes northward through the Saddle. This leaves a ca. 7 Sv contribution for the Bounty Gyre, which is ample as modern gyre transport is ca. 5 Sv [*Morris et al*., 2001]. Accordingly, and in the absence of direct volume transport measurements from Pukaki Saddle, we surmise that the contribution from that southeastern source is modest, even though it also connects directly with the gyre [*Davis*, 1998]. This is in contrast to glacial periods when marked strengthening of the ACC due to the northward migration and compression of the ACC fronts against Campbell Plateau enhances the subantarctic flow through Pukaki Saddle and northward to the North Island [*Neil et al*., 2004].

[36] Warm core eddies are a feature of the eastern North Island [*Roemmich and Sutton*, 1998; *Chiswell*, 2005]. One semipermanent recirculation, the Wairarapa Eddy, is centered near site MD97-2121 where a strong anomaly of 4.3°C is recorded. The last two decades of modern hydrographic and satellite observations show an increasing trend in sea level and dynamic height in the Wairarapa Eddy [*Chiswell*, 2005], which is in concert with increased wind stress curl over the South Pacific. Thus the increased temperatures during MIS 5e may reflect increased circulation in the Wairarapa Eddy produced by wind stress curl over the South Pacific and transmitted to the western boundary via Rossby waves [*Hill et al*., 2011]. Furthermore, the eddy may receive warm water that has leaked from the eastern South Island margin to the north via Mernoo Saddle [*Greig and Gilmour*, 1992] and potentially the Wairarapa Coastal Current [*Chiswell*, 2000]. However, why did MD97-2121 warm and P71 off northernmost New Zealand cool slightly? We can only speculate, but an additional factor is that P71 is presently sited at the cool rim of the warm core North Cape eddy [*Roemmich and Sutton*, 1998] and may not have received the full temperature signal of the boundary current that the more eddy-centered MD97-2121 would.

[37] In summary, while modern observations show an increasing trend in the circulation of the Wairarapa Eddy, transport in the East Auckland/Tasman Front has been observed to decline over the same time [*Hill et al*., 2011]. The different response in the two different regions of the boundary current may explain why the MIS 5e warming response observed in our records is much stronger in the Wairarapa Eddy compared to site P71. Alternatively, the location of the sites within eddies may be playing a role in their temperature signal.

[38] The presence of a warm pool over the central Campbell Plateau (2.4 to 4.7°C anomalies at the four sites south of the Chatham Rise) had been previously documented for glacial-interglacial conditions going back to MIS 6 [*Neil et al*., 2004]. Based on evidence from $\delta^{18}O$ of planktic foraminifera, *Globigerina bulloides* and *Globorotalia inflata*, these authors also suggest strong stratification of waters over the central Campbell Plateau during interglacial periods, and weaker stratification at the plateau margins (SO136-38) due to interaction with a vigorous ACC [*Neil et al*., 2004; *Hayward et al*., 2008]. It thus appears that the central Campbell Plateau was relatively less affected by the ACC in the south, but rather would have experienced a stronger subtropical influence (generating the observed warm anomalies) via an STF that was either located further south or had a greater volume of flow.

5.2. North Versus South Forcing—Evidence from Faunal Assemblages

[39] From the previous discussion, it is clear that there are uncertainties regarding the source(s) of ocean heat to account for some anomalies, especially those proximal to the STF where both subtropical and/or subantarctic origins are feasible. An indicator of the sources (i.e., STW or warmed SAW from the Southern Ocean) may be the presence/absence of key foraminiferal taxa that characterize polar or subtropical/tropical assemblages [e.g., *Crundwell et al*., 2008]. To further assess the contribution of different water masses to the MIS 5e circulation and heat budget, we used a ratio (Figure 4) based on the abundances of two foraminiferal planktic species (*Neogloboquadrina incompta*/*N. incompta* + *N. pachyderma*). This ratio is particularly sensitive and reflects the strong preference of *N. pachyderma* for subantarctic surface waters and thus approaches unity in MIS 5e subtropical waters of (i) the EAC and its southern extension off Tasmania and (ii) along the Tasman Front and the Auckland-East Cape currents to the eastern end of Chatham Rise (ODP 1123) (Figure 4, bottom). Thus, it appears that the general subtropical flow pathways were maintained in MIS 5e.

[40] Off the western South Island, MD06-2986 is warmed by 1.5°C together with a *N. incompta*/*N. incompta* + *N. pachyderma* of 0.97, pointing toward a subtropical source (Figure 4, bottom). This suggests that a trans-Tasman flow extended to the South Island to enhance the Southland Current feeding into the Bounty Trough. At control point DSDP 594 at the Trough head, the foraminiferal ratio reduces to 0.64 as *N. pachyderma*-bearing SAW becomes more prominent. At this location, warmest MAT-derived SSTs [*Hayward*, unpublished data] are associated with ratios of 0.78–0.79, that are likely to be affected not only by a subtropical dominant SC but also by jetting of STW water through the Mernoo Saddle [e.g., *Greig and Gilmour*, 1992; *Shaw and Vennell*, 2000]. A similar ratio of 0.61 is recorded over the South Tasman Rise just south of the STF. In full SAW, away from the STF, ratios are <0.3 except at site Y9, which may be affected by southward migrating eddies from the STF [*Williams*, 2004].

5.3. Mechanisms Affecting MIS 5e Change

5.3.1. Insights From Modern Observations and Simulations

[41] Over the last seven decades the SW Pacific Ocean and climate have responded to changes in the wind regime that ultimately appear related to the present warming phase [*Roemmich et al*., 2007; *Ridgway and Hill*, 2009; *Hill et al*., 2008, 2011]. While these modern observations occupy a minute fraction of time compared to the ca. 14 ky of MIS 5e, they are nonetheless instructive regarding the potential processes that caused change during MIS 5e.

[42] Essentially, in recent times the SPG has spun-up under strengthened subtropical westerly winds in the presence of a more positive Southern Annular Mode [*Ridgway et al*., 2008; *Thompson et al*. 2011]. The resultant increased wind stress curl over the South Pacific [*Hill et al*., 2010; *Fernandez*, 2012] has caused the EAC arm of the SPG to extend poleward by ca. 350 km as deduced from rises in temperature of ca. 1.6°C and salinity of 0.24 as measured off Tasmania since 1944 [*Hill et al*., 2008, 2010]. This marked shift to subtropical conditions was accompanied by colonizing subtropical benthic and planktic biota [*Cubillos et al*., 2007; *Hill et al*., 2008; *Ling et al*., 2009]. Such findings are consistent with our observations of enhanced warming and southward migration of subtropical planktic foraminifers in MIS 5e implying that enhanced wind curl stress was also the driving mechanism at that time albeit under natural forcings compared to today's anthropogenic influences, namely increased greenhouse gas emissions and the ozone hole [e.g., *Thompson et al*., 2011].

[43] The Tasmanian "hot spot" presently resides within the STF zone—the broad meandering dual-frontal system that links Tasmania and southernmost New Zealand [*Hamilton*, 2006]. Driven primarily by westerly winds, this complex mix of eddies, filaments, and vertically interleaved water masses transfers a ca. 3 Sv mix of STW and SAW to southernmost New Zealand [*Stramma et al*., 1995] although this volume flow is likely to increase with strengthened subtropical westerlies. The type of water mass delivered to the Campbell Plateau and South Island continental margin cannot be reconciled with modern observations, which point to times when either SAW [*Sutton*, 2003] or STW dominates [*Smith et al*., 2013].

[44] To further refine the processes driving modern change and their projected behavior, we turn to several model simulations [*Cai*, 2006; *Cai et al*., 2010; *Wu et al*., 2012]. These global models confirm the observed southward enhancement of the SPG in the presence of an increasingly positive wind stress curl. As a result, boundary currents off eastern Australia and eastern South Island become more energetic, and the interconnecting trans-Tasman flow increases. Because of the coarse model resolution, temperature trends are unclear, although *Cai et al*. [2010] reveal increased ocean heat content through the Tasman Sea and off eastern South Island.

[45] Improved resolution, captured in the eddy-resolving model simulations of *Matear et al*. [2013], allows to predict an increase in SST and eddy kinetic energy (EKE) in the Tasman Sea for the 1990s to 2060s. EKE enhancement is more or less continuous between Tasmania, southernmost New Zealand, and Campbell Plateau, and is accompanied by increased phytoplankton productivity and concentrations. This pairing is interpreted to reflect the influence of eddies, shed from the much energized EAC, that draw up nutrients from depth to nourish the surface waters of the Tasman Sea that was previously nutrient limited [*Matear et al*., 2013]. This model-based projection is consistent with our proposition of a more energetic STF link between Tasmania and the South Island during MIS 5e.

[46] In the north Tasman Sea, recent studies [*Cai et al*., 2005; *Sasaki et al*., 2008] suggest that an increase in the EAC flow does not necessarily result in a stronger flow along the Tasman Front. They propose that the southward extension of the EAC may be at the expense of the Tasman Front, whose volume transport could decline as suggested by short-term, modern observations [*Hill et al*., 2011], which cover too short time scales to be conclusive. However, a decoupled response of the Tasman Front and its eastward-directed recirculation/branches to an enhanced EAC is consistent with our paleo-data from MIS 5e, when a cooling (relative to modern conditions) is documented in the northeastern Tasman Sea, and a strong warming off the southern South Island and on the Campbell Plateau.

[47] Immediately south of the Tasman Sea, poleward shifts have been observed in all the fronts of the ACC in a circumpolar average and are presumably responding to the southward shift in the westerly winds over recent decades [*Sokolov and Rintoul*, 2009b]. However, the greatest southward frontal shifts occur in the southwest Atlantic [*Sokolov and Rintoul*, 2009b], while the fronts between subtropical and subantarctic waters in the Pacific are either difficult to identify [*Sokolov and Rintoul*, 2009a], respond differently than other basins to climate modes [*Sallée et al*., 2008], or show a strengthening but little shift in latitude over the last two decades [*Fernandez*, 2012]. While wind stress curl over the South Pacific is expected to further influence the circulation of subtropical water (and shows no southward shift over the instrumental period), the roles of wind stress, wind stress curl, and buoyancy forcing in controlling flow in the ACC (and the associated flow of subantarctic water in this region) are open questions [see for example discussion of *LaCasce and Isachsen*, 2010]. Thus, without more modern mechanistic evidence, it is unclear whether the presence of subtropical water in the Bounty Trough and over the Campbell Plateau is the result of stronger wind stress curl over the South Pacific Subtropical Gyre, a southward movement of the curl, or whether the response of the flow in the ACC to atmospheric forcing is playing a leading role, with different responses of frontal locations in each of the Southern Ocean sectors.

5.3.2. Model Simulations of MIS 5e

[48] A recent multimodel study uses 14 General Circulation Models (GCMs) and Earth system Models of Intermediate Complexity (EMICs) to provide a global SST anomaly for the early part of last interglacial (130–125 ka) relative to preindustrial time [*Lunt et al*., 2013; Figure 9]. The results of the model ensemble are also compared to a recent temperature proxy data compilation [*Turney and Jones*, 2010]. The main source of disagreement between the simulations and the proxy data is in the large LIG annual mean SST anomalies observed in the data not being replicated by the models. While the situation improves slightly when considering seasonal, rather than annual, SST change, the disagreement between modeled anomalies and the proxy data presented in *Turney and Jones* [2010] is particularly evident when considering how the data represent anomalies relative to modern (1961–1990), whereas the model simulations are relative to

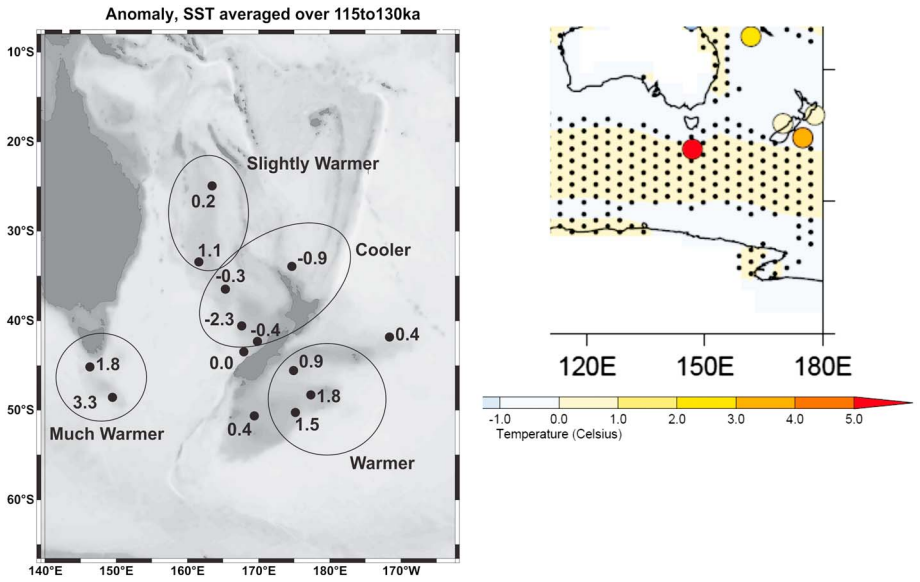

Figure 5. Geographic pattern of proxy SST anomalies (**Left Panel**: this study, averaged proxy SST in a 115 to 130 ka window minus modern mean annual SST, see details in Table 2. Note: the −2.3°C anomaly at site DSDP 593 to the west of New Zealand is probably an artefact due to the availability of only two data points at ca. 120–123 ka, substantially later, and colder, than the MIS 5 SST optimum) compared to (**Right Panel**) the proxy SST data for the same period (colored circles) from *Turney and Jones* [2010], and to the simulated anomalies (colored areas) from *Lunt et al*. [2013]. The stippled pattern represents areas where more than 70% of the models in *Lunt et al*. [2013] ensemble do not agree on the sign of the anomaly.

the (cooler) preindustrial. In order to compare our proxy data to both *Lunt et al*. [2013] and *Turney and Jones* [2010], for each of our records we averaged the SST data we had available for the 115 to 130 ka interval (Figure 5 and Table 2). Apart from the above mentioned problem with the magnitude of the signal, the general pattern of the simulated anomaly (robust cooling in the Tasman Front/East Tasman Sea, equivocal warming in the EAC region and south of the Subtropical Front) is well captured in our data (see also Figure 2). Our data also agree well with the limited (five) data points from this region from *Turney and Jones* [2010], suggesting that the warmest anomalies are located close to Tasmania, with high anomaly values on the Campbell Plateau, east of New Zealand, and in the feeding region for the EAC (southwest of New Caledonia), and either a slight cooling (our data) or warming in the Tasman Front region.

[49] The absence, in the models reviewed by *Lunt et al*. [2013], of a substantial warming to the SE of Australia and close to Tasmania (as observed in the proxy data) is probably resulting from the lack of spatial resolution, as the simulations

Table 2. Mean SST Proxy Data (This Study) Have Been Generated for the 115 to 130 ka Time Slice, in Order to Compare the Anomaly Geographic Pattern to the Results of *Turney and Jones* [2010] and *Lunt et al*. [2013][a]

Site	Proxy Mean SST	Proxy StDev SST	# of Data points	Mean LSR	StDev LSR	Observed Modern MeanSST	Anomaly Avg115to130	Anomaly Window	Anomaly at 125 ka
MD97-2106	14.43	1.08	8	7.12	0.88	12.58	**1.8**	3.55	1.72
ODP 1123	15.29	2.38	6	3.63	0.00	14.94	**0.4**	2.43	1.26
MD06-2986	14.90	1.43	6	4.03	0.15	14.93	**0.0**	1.47	1.47
Z2108	21.36	0.62	4	1.39	0.00	20.21	**1.1**	1.49	1.89
MD97-2108	12.76	1.08	5	1.78	0.00	9.49	**3.3**	4.91	3.01
P71	18.47	0.66	5	0.95	0.00	19.34	**−0.9**	−0.15	−0.74
DSDP 594	11.34	1.79	11	11.12	0.85	10.41	**0.9**	4.74	2.69
Y9	10.66	1.03	6	1.59	0.06	8.82	**1.8**	3.48	2.28
DSDP 593	13.35	2.52	2	1.87	0.01	15.61	**−2.3**	−0.48	−0.48
DSDP 592	17.43	0.23	2	0.87	0.00	17.76	**−0.3**	−0.49	−0.46
MD97-2109	9.45	2.13	6	1.98	0.34	9.05	**0.4**	2.56	0.75
SO136-038	9.45	1.78	3	0.89	0.00	8.00	**1.5**	2.41	−0.60
RC12-113	23.75	nan	1	0.85	0.00	23.55	**0.2**	0.25	0.25
SO136-003	15.13	0.39	7	nan	nan	15.55	**−0.4**	0.85	−0.45

[a]The table shows the proxy mean SST, along with its standard deviation, the number of data points we had available for this interval, the mean linear sedimentation rate and its standard deviation, the modern mean annual SST, and the resulting anomaly for the 115 to 130 ka interval (values in bold, shown in Figure 5). The anomaly values at 125 ka, and those resulting from a "window approach," i.e., picking the maximum SST value in the 120 to 132 ka window (last two columns), are those discussed throughout the text and shown in Figure 2.

are not eddy permitting. Eddy-mediated heat transport is, however, a very important mechanism in the EAC, particularly to the south of the point where the current separates from the Australian coast, as it has been recently convincingly demonstrated by the application of an eddy-resolving model to the EAC and Tasman Sea region [*Matear et al*., 2013].

6. Summary/Conclusions

[50] 1. Paleo-SSTs between 100 and 160 ka in 17 SW Pacific cores were estimated with an ensemble decision tree method (*Random Forest*) trained on 1223 Southern Hemisphere planktonic foraminiferal core-top faunas;

[51] 2. Eight new SST records have been generated for this study (Cores DSDP 592, DSDP 593, MD97-2106, P71, RC12-113, SO136-38, Y9, and Z2108) and thus add to the oceanographic database from this relatively undersampled, but influential region of the World Ocean; Oceanic SSTs in the Tasman Sea and around New Zealand were generally warmer than present, and likely occurred in the presence of a strengthened EAC that may have extended south to Tasmania to create SST anomalies of up to 4.9°C;

[52] 3. The southward extension of the EAC may have been at the expense of the Tasman Front whose volume transport to the eastern New Zealand margin may have declined. Where the Tasman Front reattaches to the eastern New Zealand margin, SSTs appear to be (i) slightly cooler (<1°C) in the inflow gateway and (ii) much warmer (>2.0°C) in the south;

[53] 4. Particularly warmer SST anomalies (2.4 to 4.7°C) are reconstructed within Bounty Trough, and appear to be mainly related to a warmer water entering from the south via the Southland Current, with possible contributions from north of the STF and subantarctic sources in the SE;

[54] 5. Recent oceanographic observations and trends indicate a strengthening of the EAC and its outflows, along with a slight cooling of the Tasman Front [*Cai et al*., 2005; *Sasaki et al*., 2008; *Hill et al*., 2011]. We also observe this geographic pattern in the MIS 5e SST anomalies. In both cases, the observed changes occur with an increase in the wind stress curl over the South Pacific

[55] **Acknowledgments.** This research was supported financially by a Foundation for Research, Science, and Technology (FRST) Grant (GD, LC) and by the Global Change through Time (GCT) Program at GNS Science (GC, GS, MC). We would like to thank Patrick DeDeckker (ANU) for tracking down foraminiferal census data and samples in The Australian National University archives, Michal Kucera (University of Tübingen) for granting access to the MARGO data set, and two anonymous reviewers, whose comments greatly improved the final manuscript.

References

Barrows, T. T., S. Juggins, P. De Deckker, E. Calvo, and C. Pelejero (2007), Long-term sea surface temperature and climate change in the Australian–New Zealand region, *Paleoceanography*, *22*, PA2215, doi:10.1029/2006PA001328.

Bé, A. W. H. (1977), An ecological, zoogeographic and taxonomic review of Recent planktonic foraminifera, in *Oceanic Micropaleontology*, edited by A. T. S. Ramsay, pp. 1–100, Academic Press, London.

Bi, J., and K. Bennett (2003), Regression error characteristic curves, in *Proceedings of the Twentieth International Conference on Machine Learning*, edited, pp. 43–50, Washington, DC.

Bianchi, C., and R. Gersonde (2002), The Southern Ocean surface between Marine Isotope Stages 6 and 5d: shape and timing of climate changes, *Palaeogeogr. Palaeoclimatol. Palaeoecol.*, *187*, 151–177.

Birks, H. J. B., O. Heiri, H. Seppä, and A. E. Bjune (2010), Strengths and weaknesses of quantitative climate reconstructions based on Late-Quaternary biological proxies, *The Open Ecology Journal*, *3*, 68–110.

Bowen, M. M., J. L. Wilkin, and W. J. Emery (2005), Variability and forcing of the East Australian Current, *J. Geophys. Res.*, *110*, C03019, doi:10.1029/2004JC002533.

Breiman, L. (2001), Random Forests, *Machine Learning*, *45*, 5–32.

Cai, W. (2006), Antarctic ozone depletion causes an intensification of the Southern Ocean super-gyre circulation, *Geophys. Res. Lett.*, *33*, L03712, doi:10.1029/2005GL024911.

Cai, W., G. Shi, T. Cowan, D. Bi, and J. Ribbe (2005), The response of the Southern Annular Mode, the East Australian Current, and the southern mid-latitude ocean circulation to global warming, *Geophys. Res. Lett.*, *32*, L23706, doi:10.1029/2005GL024701.

Cai, W., T. Cowan, G. Stuart, and S. Wijffels (2010), Simulations of processes associated with the fast warming rate of the Southern midlatitude Ocean, *J. Clim.*, *23*, 197–206.

Carter, L., R. D. Garlick, P. Sutton, S. Chiswell, N. A. Oien, and B. R. Stanton (1998), Ocean Circulation New Zealand, *NIWA Chart Miscellaneous Series*, *76*.

Carter, L., B. Manighetti, G. Ganssen, and L. Northcote (2008), Southwest Pacific modulation of abrupt climate change during the Antarctic Cold Reversal–Younger Dryas, *Palaeogeogr. Palaeoclimatol. Palaeoecol.*, *260*, 284–298.

Chiswell, S. M. (2000), The Wairarapa Coastal Current, *N.Z. J. Mar. Freshwater Res.*, *34*, 303–315.

Chiswell, S. M. (2005), Mean and variability in the Wairarapa and Hikurangi eddies, *N.Z. J. Mar. Freshwater Res.*, *39*, 121–134.

CLIMAP (Climate: Long Range Investigation, Mapping, and Prediction) Project Members (1976), The surface of the ice-age earth, *Science*, *191*, 1131–1137.

CLIMAP (Climate: Long Range Investigation, Mapping, and Prediction) Project Members (1981), Seasonal reconstructions of the Earth's surface at the Last Glacial Maximum, *Geological Society of America*, *Map and Chart Series*, *MC-36*.

CLIMAP (Climate: Long Range Investigation, Mapping, and Prediction) Project Members (1984), The Last Interglacial ocean, *Quat. Res.*, *21*, 123–224.

Cortez, P. (2010), Data Mining with Neural Networks and Support Vector Machines using the R/rminer Tool, in *Advances in Data Mining - Applications and Theoretical Aspects,10th Industrial Conference on Data Mining, LNAI 6171*, edited by P. Perner, pp. 572–583, Springer, Berlin, Germany.

Crundwell, M., G. Scott, T. Naish, and L. Carter (2008), Glacial–interglacial ocean climate variability from planktonic foraminifera during the Mid-Pleistocene transition in the temperate Southwest Pacific, ODP Site 1123, *Palaeogeogr. Palaeoclimatol. Palaeoecol.*, *260*, 202–229.

Cubillos, J., S. Wright, G. Nash, M. de Salas, B. Griffiths, B. Tilbrook, A. Poisson, and G. M. Hallegraeff (2007), Calcification morphotypes of the coccolithophorid *Emiliania huxleyi* in the Southern Ocean: Changes in 2001 to 2006 compared to historical data, *Mar. Ecol. Prog. Ser.*, *348*, 47–54.

Davis, R. (1998), Preliminary results from directly measuring mid-depth circulation in the tropical and South Pacific, *J. Geophys. Res.*, *103*, 24,619–24,639.

Fernandez, D. (2012), Do winds control the confluence of subtropical and subantarctic surface waters east of New Zealand? M.Sc. thesis, 90 pp, Victoria University of Wellington, Wellington.

Gille, S. T. (2002), Warming of the Southern Ocean since the 1950s, *Science*, *295*, 1275–1277.

Gille, S. T. (2008), Decadal-scale temperature trends in the Southern Hemisphere Ocean, *J. Clim.*, *21*, 4749–4765.

Greig, M. J., and A. J. Gilmour (1992), Flow through the Mernoo Saddle, New Zealand, *N.Z. J. Mar. Freshwater Res.*, *26*, 155–165.

Hall, I. R., I. N. McCave, N. J. Shackleton, G. P. Weedon, and S. E. Harris (2001), Intensified deep Pacific inflow and ventilation in Pleistocene glacial times, *Nature*, *412*, 809–812.

Hamilton, L. J. (2006), Structure of the Subtropical Front in the Tasman Sea, *Deep Sea Res., Part I*, *53*, 1989–2009.

Hastie, T., R. Tibshirani, and J. Friedman (2009), *The Elements of Statistical Learning*, 746 pp., Springer-Verlag, New York.

Hayward, B. W., et al. (2008), The effect of submerged plateaux on Pleistocene gyral circulation and sea-surface temperatures in the Southwest Pacific, *Global Planet. Change*, *63*, 309–316, doi:10.1016/j.gloplacha.2008.07.003.

Hayward, B. W., et al. (2012), Planktic foraminifera-based sea-surface temperature record in the Tasman Sea and history of the Subtropical Front around New Zealand, over the last one million years, *Mar. Micropaleontol.*, *82-83*, 13–27.

Head, P. S., and C. S. Nelson (1994), A high-resolution oxygen isotope record for the past 6.4 million years at DSDP Site 593, Challenger Plateau, southern Tasman Sea, in *Evolution of the Tasman Sea Basin*, edited by G. J. van der Lingen et al., pp. 159–179, A.A. Balkema, Rotterdam.

Hill, K. L., S. R. Rintoul, R. Coleman, and K. R. Ridgway (2008), Wind forced low frequency variability of the East Australian Current, *Geophys. Res. Lett.*, *35*, L08602, doi:10.1029/2007/GL032912.

Hill, K. L., S. R. Rintoul, P. R. Oke, and K. Ridgway (2010), Rapid response of the East Australian Current to remote wind forcing: The role of barotropic-baroclinic interactions, *J. Mar. Res.*, *68*, 413–431.

Hill, K. L., S. R. Rintoul, K. R. Ridgway, and P. R. Oke (2011), Decadal changes in the South Pacific western boundary current system revealed in observations and ocean state estimates *J. Geophys. Res.*, *116*, C01009, doi:10.1029/2009JC005926.

Howard, W. R., and W. L. Prell (1984), A comparison of radiolarian and foraminiferal paleoecology in the Southern Indian Ocean: new evidence for the interhemispheric timing of climatic change, *Quat. Res.*, *21*, 244–263, doi:10.1016/0033-5894(84)90100-5.

Howard, W. R., and W. L. Prell (1992), Late Quaternary surface circulation of the Southern Indian Ocean and its relationship to orbital variations, *Paleoceanography*, *7*, 79–117.

Hutson, W. H. (1980), The Agulhas current during the late Pleistocene: Analysis of modern faunal analogs, *Science*, *207*, 64–66.

Imbrie, J., and N. G. Kipp (1971), A new micropaleontological method for quantitative paleoclimatology: Application to a late Pleistocene Caribbean core, in *Late Cenozoic Glacial Ages*, edited by K. Turekian, pp. 71–181, Yale University Press, New Haven, Connecticut.

Kalnay, E., et al. (1996), The NCEP/NCAR 40-year Reanalysis Project, *Bull. Am. Meteorol. Soc.*, *77*(3), 437–471.

Kolodziej, A. P. (2010), Planktic foraminifera-based sea surface temperature estimates and Late Quaternary oceanography off New Zealand's West Coast, M.Sc. thesis, Victoria University of Wellington, Wellington, New Zealand.

Kucera, M., et al. (2005), Reconstruction of sea-surface temperatures from assemblages of planktonic foraminifera: multi-technique approach based on geographically constrained calibration data sets and its application to glacial Atlantic and Pacific Oceans, *Quat. Sci. Rev.*, *24*, 951–998.

LaCasce, J. H., and P. E. Isachsen (2010), The linear models of the ACC, *Prog. Oceanogr.*, *84*, 139–157, doi:10.1016/j.pocean.2009.11.002.

Leduc, G., R. Schneider, J.-H. Kim, and G. Lohmann (2010), Holocene and Eemian sea surface temperature trends as revealed by alkenone and Mg/Ca paleothermometry, *Quat. Sci. Rev.*, *29*, 989–1004, doi:10.1016/j.quascirev.2010.01.004.

Liaw, A., and M. Wiener (2002), Classification and Regression by randomForest, *R News*, *2*(3), 18–22.

Ling, S. D., C. R. Johnson, K. Ridgway, A. J. Hobday, and M. Haddon (2009), Climate-driven range extension of a sea urchin: inferring future trends by analysis of recent population dynamics, *Global Change Biol.*, *15*, 719–731.

Lisiecki, L. E., and M. E. Raymo (2005), A Pliocene-Pleistocene stack of 57 globally distributed benthic $\delta^{18}O$ records, *Paleoceanography*, *20*, PA1003, doi:10.1029/2004PA001071.

Loutre, M. F., and A. Berger (2003), Marine Isotope Stage 11 as an analogue for the present interglacial, *Global Planet. Change*, *36*, 209–217.

Lunt, D. J., et al. (2013), A multi-model assessment of last interglacial temperatures, *Climate of the Past*, *9*, 699–717.

Malmgren, B. A., and U. Nordlund (1997), Application of artificial neural networks to paleoceanographic data, *Palaeogeogr. Palaeoclimatol. Palaeoecol.*, *136*, 359–373.

Malmgren, B. A., M. Kucera, J. Nyberg, and C. Waelbroeck (2001), Comparison of statistical and artificial neural network techniques for estimating past sea surface temperatures from planktonic foraminifer census data, *Paleoceanography*, *16*(5), 1–11.

MARGO Project Members (2009), Constraints on the magnitude and patterns of ocean cooling at the Last Glacial Maximum, *Nat. Geosci.*, *2*, 127–132, doi:10.1038/ngeo411.

Martinez, J. I. (1994), Late Pleistocene palaeoceanography of the Tasman Sea: Implications for the dynamics of the warm pool in the western Pacific, *Palaeogeogr. Palaeoclimatol. Palaeoecol.*, *112*, 19–62.

Matear, R. J., M. A. Chamberlain, C. Sun, and M. Feng (2013), Climate change projection of the Tasman Sea from an eddy resolving model, *J. Geophys. Res. Oceans*, *118*, 1–16.

Mohtadi, M., D. Hebbeln, and M. Marchant (2005), Upwelling and productivity along the Peru-Chile Current derived from faunal and isotopic compositions of planktic foraminifera in surface sediments, *Mar. Geol.*, *216*(3), 107–126.

Mohtadi, M., L. Max, D. Hebbeln, A. Baumgart, N. Krück, and T. Jennerjahn (2007), Modern environmental conditions recorded in surface sediment samples off W and SW Indonesia: Planktonic foraminifera and biogenic compounds analyses, *Mar. Micropaleontol.*, *65*(1–2), 96–112.

Morris, M., B. R. Stanton, and H. L. Neil (2001), Subantarctic oceanography around New Zealand: preliminary results from an ongoing survey, *N.Z. J. Mar. Freshwater Res.*, *35*, 499–519.

Moy, A. D., W. R. Howard, and M. K. Gagan (2006), Late Quaternary palaeoceanography of the Circumpolar Deep Water from the South Tasman Rise, *Journal of Quaternary Science*, *21*(7), 763–777, doi:10.1002/jqs.1067.

Neil, H. L., L. Carter, and M. Y. Morris (2004), Thermal isolation of Campbell Plateau, New Zealand, by the Antarctic Circumpolar Current over the past 130 kyr, *Paleoceanography*, *19*, PA4008, doi:10.1029/2003PA000975.

Nelson, C. S., P. J. Cooke, C. H. Hendy, and A. M. Cuthbertson (1993), Oceanographic and climatic changes over the past 160,000 years at Deep Sea Drilling Project Site 594 off southeastern New Zealand, southwest Pacific Ocean, *Paleoceanography*, *8*(4), 435–458.

Nelson, C. S., C. H. Hendy, and A. M. Cuthbertson (1994), Oxygen isotope evidence for climatic contrasts between Tasman Sea and Southwest Pacific Ocean during the late Quaternary, in *Evolution of the Tasman Sea Basin*, edited by G. J. van der Lingen et al., pp. 181–196, A.A. Balkema, Rotterdam.

Nürnberg, D., and J. Groeneveld (2006), Pleistocene variability of the Subtropical Convergence at East Tasman Plateau: Evidence from planktonic foraminiferal Mg/Ca (ODP Site 1172A), *Geochemistry, Geophysics, Geosystems*, *7*, Q04P11, doi:10.1029/2005GC000984.

Orsi, A., and U. Harris (2001), Locations of the various fronts in the Southern Ocean, *Australian Antarctic Data Centre - CAASM Metadata*. (http://gcmd.nasa.gov/KeywordSearch/Metadata.do?Portal=amd_au&MetadataView=Full&MetadataType=0&KeywordPath=&OrigMetadataNode=AADC&EntryId=southern_ocean_fronts).

Orsi, A. H., T. Whitworth III, and W. D. Nowlin Jr. (1995), On the meridional extent and fronts of the Antarctic Circumpolar Current, *Deep Sea Res.*, *42*(5), 641–673.

Paillard, D., L. Labeyrie, and P. Yiou (1996), Macintosh program performs time-series analysis, *Eos Transactions AGU*, *77*, 379, doi:10.1029/96EO00259.

Ridgway, K. R., and J. R. Dunn (2003), Mesoscale structure of the mean East Australian Current System and its relationship with topography, *Prog. Oceanogr.*, *56*, 189–222.

Ridgway, K. R., and J. R. Dunn (2007), Observational evidence for a Southern Hemisphere oceanic supergyre, *Geophys. Res. Lett.*, *34*, L13612, doi:10.1029/2007GL030392.

Ridgway, K., and K. Hill (2009), The East Australian Current, in *A Marine Climate Change Impacts and Adaptation Report Card for Australia 2009*, edited by E. S. Poloczanska et al., 1–6, CSIRO (The Commonwealth Scientific and Industrial Research Organization), Clayton, Australia.

Ridgway, K. R., J. R. Dunn, and J. L. Wilkin (2002), Ocean interpolation by four-dimensional least squares - Application to the waters around Australia, *J. Atmos. Oceanic Technol.*, *19*(9), 1357–1375.

Ridgway, K. R., R. C. Coleman, R. J. Bailey, and P. Sutton (2008), Decadal variability of East Australian Current transport inferred from repeated high-density XBT transects, a CTD survey and satellite altimetry, *J. Geophys. Res.*, *113*, C08039, doi:10.1029/2007JC004664.

Rintoul, S., and S. Sokolov (2001), Baroclinic transport variability of the Antarctic Circumpolar Current south of Australia (WOCE repeat section SR3), *J. Geophys. Res.*, *106*(C2), doi:10.1029/2000JC900107.

Roemmich, D., and P. J. H. Sutton (1998), The mean and variability of ocean circulation past northern New Zealand: determining the representativeness of hydrographic climatologies, *J. Geophys. Res.*, *103*(C6), 13,041–13,054.

Roemmich, D., J. Gilson, R. Davis, P. Sutton, S. Wijffels, and S. Riser (2007), Decadal spinup of the South Pacific Subtropical Gyre, *J. Phys. Oceanogr.*, *37*, 162–173.

Sallée, J. B., K. Speer, and R. Morrow (2008), Southern Ocean fronts and their variability to climate modes, *J. Clim.*, *21*(12), 3020–3039, doi:10.1175/2007JCLI1702.1.

Sasaki, H., M. Nonaka, Y. Masumoto, Y. Sasai, H. Uehara, and H. Sakuma (2008), An eddy-resolving hindcast simulation of the quasi-global ocean from 1950 to 2003 on the Earth Simulator, in *High resolution numerical modeling of the atmosphere and ocean*, edited by K. Hamilton and W. Ohfuchi, pp. 157–186, Springer, New York.

Shaw, A. G. P., and R. Vennell (2000), Variability of water masses through the Mernoo Saddle, South Island, New Zealand, *N.Z. J. Mar. Freshwater Res.*, *34*, 103–116.

Sikes, E. L., W. R. Howard, H. L. Neil, and J. K. Volkman (2002), Glacial-interglacial sea surface temperature changes across the subtropical front east of New Zealand based on alkenone unsaturation ratios and foraminiferal assemblages, *Paleoceanography*, *17*(2), 1012, doi:10.1029/2001PA000640.

Sikes, E. L., W. R. Howard, C. R. Samson, T. S. Mahan, L. G. Robertson, and J. K. Volkman (2009), Southern Ocean seasonal temperature and Subtropical Front movement on the South Tasman Rise in the late Quaternary, *Paleoceanography*, *24*, PA2201, doi:10.1029/2008PA001659.

Smith, R. O., R. Vennell, H. C. Bostock, and M. J. M. Williams (2013), Interaction of the subtropical front with topography around southern New Zealand, *Deep Sea Res., Part I*, *76*, 13–26.

Sokolov, S., and S. R. Rintoul (2009a), Circumpolar structure and distribution of the Antarctic Circumpolar Current fronts. Part 2: Variability and relationship to sea surface height, *J. Geophys. Res.*, *114*, C11019, doi:10.1029/2008JC005248.

Sokolov, S., and S. R. Rintoul (2009b), Circumpolar structure and distribution of the Antarctic Circumpolar Current fronts. Part 1: Mean circumpolar paths, *J. Geophys. Res.*, *114*, C11018, doi:10.1029/2008JC005108.

Stanton, B. R. (2001), Estimating the East Auckland Current transport from model winds and the Island Rule, *N.Z. J. Mar. Freshwater Res.*, *35*(3), 531–540.

Stanton, B. R., and M. Morris (2004), Direct velocity measurements in the Subantarctic Front and over Campbell Plateau, south-east of New Zealand, *J. Geophys. Res.*, *109*, C01028, doi:10.1029/2002JC001339.

Stanton, B. R., P. J. H. Sutton, and S. M. Chiswell (1997), The East Auckland Current, 1994-95, *N.Z. J. Mar. Freshwater Res.*, *31*, 537–549.

Stramma, L., R. G. Peterson, and M. Tomczak (1995), The South Pacific Current, *J. Phys. Oceanogr.*, *25*, 77–91.

Sturm, A. (2004), Changes in ocean circulation and carbonate chemistry in the Australian sector of the Southern Ocean during the last 500,000 years, Ph.D. thesis, Christian-Albrechts-Universität, Kiel, Germany.

Sutton, P. J. H. (2003), The Southland Current: A subantarctic current, *N.Z. J. Mar. Freshwater Res.*, *37*, 645–652.

Tachikawa, K., L. Vidal, C. Sonzogni, and E. Bard (2009), Glacial/interglacial sea surface temperature changes in the Southwest Pacific ocean over the past 360 ka, *Quat. Sci. Rev.*, *28*, 1160–1170.

Theron, R., D. Paillard, E. Cortijo, J. A. Flores, M. Vaquero, F. J. Sierro, and C. Waelbroeck (2004), Rapid reconstruction of paleoenvironmental features using a new multiplatform program, *Micropaleontology*, *50*, 391–395.

Thompson, W. G., and S. L. Goldstein (2006), A radiometric calibration of the SPECMAP timescale, *Quat. Sci. Rev.*, *25*, 3207–3215.

Thompson, D. W. J., S. Solomon, P. J. Kushner, M. H. England, K. M. Grise, and D. J. Karoly (2011), Signatures of the Antarctic ozone hole in Southern Hemisphere surface climate change, *Nat. Geosci.*, *4*, 741–749.

Tilburg, C. E., H. E. Hurlburt, J. J. O'Brien, and J. F. Shriver (2001), The dynamics of the East Australian Current system: The Tasman Front, the East Auckland Current, and the East Cape Current, *J. Phys. Oceanogr.*, *31*, 2917—2943.

Toggweiler, J. R., J. L. Russell, and S. R. Carson (2006), Midlatitude westerlies, atmospheric CO_2, and climate change, *Paleoceanography*, *21*, PA2005, doi:10.1029/2005PA001154.

Turney, C. S. M., and R. T. Jones (2010), Does the Agulhas Current amplify global temperatures during super-interglacials?, *Journal of Quaternary Science*, *25*, 839–843.

Tzedakis, P. C. (2010), The MIS 11 – MIS1 analogy, southern European vegetation atmospheric methane and the early anthropogenic hypothesis, *Climate of the Past*, *6*, 131–144.

Uddstrom, M. J., and N. A. Oien (1999), On the use of high resolution satellite data to describe the spatial and temporal variability of sea surface temperatures in the New Zealand region, *J. Geophys. Res.*, *104*, 20,729–20,751.

Williams, M. J. (2004), Analysis of quasi-synoptic eddy observations in the New Zealand subantarctic, *N.Z. J. Mar. Freshwater Res.*, *38*, 183–194.

Wu, L., et al. (2012), Enhanced warming over the global subtropical western boundary currents, *Nat. Clim. Change*, *2*, 161–166.